Supporting Information

Rational Optimization of Mechanism-Based Inhibitors Through Determination of the Microscopic Rate Constants of Inactivation

Carter Eiden,[ϡ] Kimberly M. Maize,[ϡ] Barry C. Finzel,[ϡ] John D. Lipscomb,[§]* Courtney C. Aldrich[ϡ,]*

[ϡ]Department of Medicinal Chemistry, University of Minnesota, Minnesota 55455, United States

[§]Department of Biochemistry, Molecular Biology, and Biophysics, University of Minnesota, Minnesota 55455, United States

*To whom correspondence should be addressed: aldri015@umn.edu, lipsc001@umn.edu

Table of Contents

I. Kinetic Analysis of Common MBI Mechanisms S-2

Table S1 ..... S-4

Table S2 ..... S-5

II. Stopped-Flow Analysis of the Inhibition of BioA by **1** S-9

Figure S1 ..... S-11

Figure S2 ..... S-12

Table S3 ..... S-13

Figure S3 ..... S-14

Table S4 ..... S-15

Table S5 ..... S-15

III. Inhibition of BioA by **2** S-16

Figure S4 ..... S-17

Figure S5 ..... S-18

IV. Crystallographic Data S-19

Table S6 ..... S-20

Figure S6 ..... S-21

V. NMR Spectra of **2** S-22

VI. References S-23

I. Kinetic analysis of common MBI mechanisms.

The k_{inact} of a MBI is defined as the maximum k_{obs} possible arising from infinite concentration of inhibitor, where k_{obs} is determined by fitting curves describing time-dependent formation of the final, inactivated complex, to exponentials of the type e^(-k_{obs}*t). K_I is the concentration of inhibitor that produces a k_{obs} equal to half of k_{inact}. To the best of our knowledge, the K_I and k_{inact} values have not been described as functions of individual microscopic rate constants for most kinetic mechanisms. To bridge this gap, we have derived values for K_I and k_{inact} for a wide variety of observed and potential mechanisms for MBIs, which are shown in **Table S1.** A sample derivation for a single mechanism is provided at the end of this section along with all of the assumptions necessary.

The addition of more steps or reversibility causes K_I and k_{inact} to become significantly more complex congregates of the microscopic rate constants. Though this table provides a wealth of valuable information, we wanted to explore exactly how the K_I and k_{inact} values depend on the individual rate constants in greater detail. K_I and k_{inact} were thus calculated from a wide range of values for each of the individual rate constants for a few mechanisms. These results are shown in **Table S2**.

It is often naively assumed that a K_I value obtained experimentally for an MBI will estimate the K_D of the initial binding step with a high degree of fidelity. This is unequivocally shown to be not true, as the K_I only accurately estimates the K_D of the initial binding event when the step following binding is both irreversible and rate limiting. In every other case, the K_I underestimates the K_D, and often by a substantial margin (light blue, purple, green, and gray entries in **Table S2**). Since a significant number of MBIs will certainly inactivate enzymes through mechanisms where the second step is either reversible or non-rate limiting, it is unwise to assume without further information that K_I estimates K_D. The distinction between K_I and K_D is important because the K_D, not the K_I, determines how well an inhibitor will compete with the substrate for binding to the enzyme active site.

The distinction between the two is further demonstrated by the observation that if the second step is irreversible and non-rate limiting, an increase in the speed of the rate limiting step will cause an increase

in both the K_I and the k_{inact} values (light blue and purple entries in **Table S2**). Clearly, improving the rate of a step subsequent to an irreversible second step does not affect the K_D of the initial binding event whatsoever, but it does cause significant changes in the K_I value. This point calls into question k_{inact}/K_I as a consistently accurate measure of inactivation efficiency. An MBI with the rate constants in the second purple entry of **Table S2** is clearly a better inhibitor than an MBI with the rate constants in the first purple entry. It would compete with substrate substantially better, but its k_{inact}/K_I value is only about 10% improved. This point is not to say that k_{inact}/K_I is a useless constant (it is certainly not), but rather to illustrate that it has pitfalls if treated as a complete descriptor of inactivation efficiency.

A final point that is demonstrated from the results in **Table S2** is that, if the second step is reversible, improving the equilibrium of this step increases the k_{inact} and lowers the K_I at the same time. This is not unexpected, as the extended reversibility would affect the apparent K_D of binding, if not the K_D of the initial binding event itself. Still, this result is one of the reasons that extensive kinetic analysis of an MBI could prove valuable; it reveals which steps are reversible/irreversible and even which steps are kinetically important. If the second step is reversible, a 5-fold improvement of its equilibrium results in around a 25-fold improvement in inhibitory potency (assumes a rapid equilibrium for the second step).

Table S1. K_I and k_{inact} values for several mechanisms of MBIs as conglomerates of rate constants.[i]

#	Mechanism:	K_I (M)	k_{inact} (s^{-1})
1	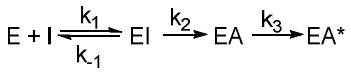	$\frac{(k_{-1}+k_2)k_3}{k_1(k_2+k_3)}$	$\frac{k_2k_3}{k_2+k_3}$
2	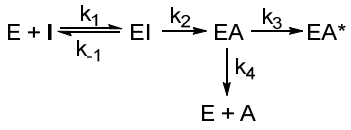	$\frac{(k_{-1}+k_2)(k_3+k_4)}{k_1(k_2+k_3+k_4)}$	$\frac{k_2k_3}{k_2+k_3+k_4}$
3	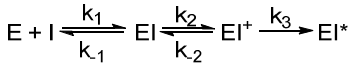	$\frac{k_{-1}(k_{-2}+k_3)+k_2k_3}{k_1(k_2+k_{-2}+k_3)}$	$\frac{k_2k_3}{k_2+k_{-2}+k_3}$
4	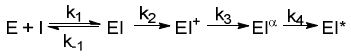	$\frac{(k_{-1}+k_2)k_3k_4}{k_1(k_2(k_3+k_4)+k_3k_4)}$	$\frac{k_2k_3k_4}{k_2(k_3+k_4)+k_3k_4}$
5	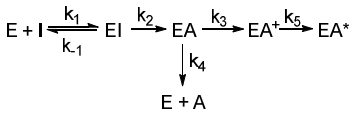	$\frac{(k_{-1}+k_2)k_3k_5+k_4k_5}{k_1(k_2(k_3+k_5)+k_5(k_3+k_4))}$	$\frac{k_2k_3k_5}{k_2(k_3+k_5)+k_5(k_3+k_4)}$
6	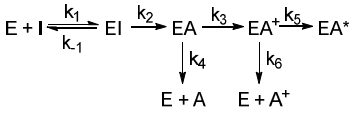	$\frac{(k_{-1}+k_2)(k_3+k_4)(k_5+k_6)}{k_1(k_2(k_3+k_5+k_6)+(k_3+k_4)(k_5+k_6))}$	$\frac{k_2k_3k_5}{k_2(k_3+k_5+k_6)+(k_3+k_4)(k_5+k_6)}$
7	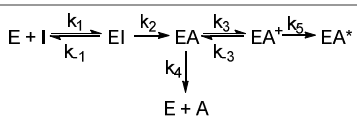	$\frac{(k_{-1}+k_2)(k_3k_5+k_{-3}k_4+k_4k_5)}{k_1(k_2(k_3+k_{-3}+k_5)+k_3k_5+k_4(k_{-3}+k_5))}$	$\frac{k_2k_3k_5}{k_2(k_3+k_{-3}+k_5)+k_3k_5+k_4(k_{-3}+k_5)}$
8	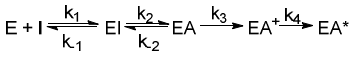	$\frac{(k_{-1}k_{-2}+k_{-1}k_3+k_2k_3)(k_4)}{k_1(k_2k_3+(k_2+k_{-2}+k_3)(k_4))}$	$\frac{k_2k_3k_4}{k_2k_3+(k_2+k_{-2}+k_3)(k_4)}$
9	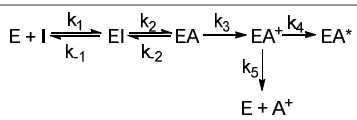	$\frac{(k_{-1}k_{-2}+k_{-1}k_3+k_2k_3)(k_4+k_5)}{k_1(k_2k_3+(k_2+k_{-2}+k_3)(k_4+k_5))}$	$\frac{k_2k_3k_4}{k_2k_3+(k_2+k_{-2}+k_3)(k_4+k_5)}$

[i] The result in #2 has been explicitly shown (Ref. 2), and the result in #1 can be easily derived from this by setting k_4 to 0. The remaining results are novel to the best of our knowledge, and we thank Kathleen Wang for independently verifying each result.

Table S2. Effect of Changing the Rate Constants on K_I, k_{inact}, and K_D.

Mech#	k_1 ($\mu M^{-1}s^{-1}$)	k_{-1} (s^{-1})	k_2 (s^{-1})	k_{-2} (s^{-1})	k_3 (s^{-1})	k_4 (s^{-1})	k_5 (s^{-1})	K_D (μM)	K_I (μM)	k_{inact} (s^{-1})	k_{inact}/K_I ($\mu M^{-1}s^{-1}$)
2	5	50	5	N/A	0.2	0.05	N/A	10	0.52	0.19	0.37
2	5	50	5	N/A	2	0.05	N/A	10	3.20	1.42	0.44
2	80	80	5	N/A	0.2	0.05	N/A	1	0.05	0.19	3.8
2	20	100	1	N/A	1	1	N/A	5	3.37	0.33	0.097
2	20	100	1	N/A	10	1	N/A	5	4.63	0.83	0.18
2	20	100	10	N/A	1	1	N/A	5	0.92	0.83	0.90
2	20	100	1	N/A	1	0.1	N/A	5	2.65	0.95	0.36
2	80	40	1	N/A	1	1	N/A	1	0.34	0.33	0.97
2	5	50	0.03	N/A	1	0.2	N/A	10	9.76	0.024	0.0025
2	5	50	0.3	N/A	1	0.2	N/A	10	8.04	0.20	0.024
2	30	30	0.03	N/A	1	0.2	N/A	1	0.98	0.024	0.024
2	100	500	10	N/A	0.05	0.01	N/A	5	0.030	0.050	1.7
2	100	500	10	N/A	0.5	0.01	N/A	5	0.25	0.48	1.9
2	100	500	10	N/A	0.05	0.001	N/A	5	0.026	0.050	1.9
3	5	50	5	0.5	0.05	N/A	N/A	10, *0.91*	1.00	0.045	0.045
3	5	50	5	0.5	0.5	N/A	N/A	10, *0.91*	1.75	0.42	0.24
3	80	80	5	0.5	0.05	N/A	N/A	1, *0.091*	0.10	0.045	0.45
3	20	100	0.03	3	0.5	N/A	N/A	5, *4.95*	4.96	0.0042	0.00085
3	20	100	0.3	3	0.5	N/A	N/A	5, *4.5*	4.61	0.039	0.0085
3	20	100	0.3	0.3	5	N/A	N/A	5, *2.5*	4.75	0.27	0.057
3	20	100	3	3	0.5	N/A	N/A	5, *2.5*	2.70	0.23	0.085
3	20	100	30	3	0.5	N/A	N/A	5, *0.45*	0.54	0.45	0.83
5	5	50	1	N/A	1	0.3	1	10	4.01	0.30	0.075
5	5	50	10	N/A	1	0.3	1	10	0.73	0.88	1.2
5	5	50	1	N/A	10	0.3	1	10	4.93	0.88	0.18
5	5	50	1	N/A	1	3	1	10	6.80	0.17	0.025
5	5	50	1	N/A	1	0.3	10	10	4.01	0.30	0.075
5	5	50	1	N/A	1	0.3	0.02	10	0.25	0.019	0.076
5	5	50	1	N/A	1	0.3	0.2	10	1.82	0.14	0.077

The numbers in italics for results obtained for mechanism 3 arise from applying the rapid equilibrium assumption to the second step as well as the first step and obtaining a K_D that is more consistent with how the inhibitor would compete with substrate. This number is a fair estimate for the green entries, and the top and bottom dark blue ones.

Derivation of the K_I and k_{inact} values for mechanism 4 in table S1.[1,2,3]

This is written for the following mechanism:

$$E + I \underset{k_{-1}}{\overset{k_1}{\rightleftharpoons}} EI \xrightarrow{k_2} EA \xrightarrow{k_3} EB \xrightarrow{k_4} EP$$

The labels for the intermediate and final complexes are changed to allow for simple writing with Word's equation editor. K_I and k_{inact} are defined as they are in **Table S1**, and the assumptions necessary are the quasi-steady state assumption for each intermediate Enzyme-Inhibitor complex and that the total enzyme concentration stays constant.

$$\frac{d[EP]}{dt} = k_4[EB]$$

$$\frac{d[EB]}{dt} = k_3[EA] - k_4[EB] = 0$$

$$\frac{d[EA]}{dt} = k_2[EI] - k_3[EA] = 0$$

$$\frac{d[EI]}{dt} = k_1[E][I] - (k_2 + k_{-1})[EI] = 0$$

$$[E]_0 = [E] + [EI] + [EA] + [EB] + [EP] = constant$$

We express [EI] in terms of the other variables:

$$k_1([E]_0 - [EI] - [EA] - [EB] - [EP])[I] - (k_2 + k_{-1})[EI] = 0$$

$$k_1([E]_0 - [EA] - [EB] - [EP])[I] = (k_2 + k_{-1})[EI] + k_1[EI][I]$$

$$([E]_0 - [EA] - [EB] - [EP])[I] = \frac{(k_2 + k_{-1})[EI]}{k_1} + [EI][I]$$

Letting $K_M = (k_2 + k_{-1})/k_1$:

$$([E]_0 - [EA] - [EB] - [EP])[I] = [EI](K_M + [I])$$

$$\frac{([E]_0 - [EA] - [EB] - [EP])[I]}{(K_M + [I])} = [EI]$$

Solving for [EA]:

$$k_2[EI] - k_3[EA] = 0$$

$$k_2 \frac{([E]_0 - [EA] - [EB] - [EP])[I]}{(K_M + [I])} - k_3[EA] = 0$$

$$k_2 \frac{([E]_0 - [EB] - [EP])[I]}{(K_M + [I])} = k_2 \frac{[EA][I]}{(K_M + [I])} + k_3[EA]$$

$$k_2 \frac{([E]_0 - [EB] - [EP])[I]}{(K_M + [I])} = (k_2 \frac{[I]}{(K_M + [I])} + k_3)[EA]$$

$$k_2 \frac{([E]_0 - [EB] - [EP])[I]}{(K_M + [I])(k_2 \frac{[I]}{(K_M + [I])} + k_3)} = [EA]$$

$$k_2 \frac{([E]_0 - [EB] - [EP])[I]}{k_2[I] + k_3(K_M + [I])} = [EA]$$

Now, we solve for [EB]

$$k_3[EA] - k_4[EB] = 0$$

$$k_2 k_3 \frac{([E]_0 - [EB] - [EP])[I]}{k_2[I] + k_3(K_M + [I])} - k_4[EB] = 0$$

$$k_2 k_3 \frac{([E]_0 - [EP])[I]}{k_2[I] + k_3(K_M + [I])} = k_2 k_3 \frac{[EB][I]}{k_2[I] + k_3(K_M + [I])} + k_4[EB]$$

$$k_2 k_3 \frac{([E]_0 - [EP])[I]}{k_2[I] + k_3(K_M + [I])} = (k_2 k_3 \frac{[I]}{k_2[I] + k_3(K_M + [I])} + k_4)[EB]$$

$$k_2 k_3 \frac{([E]_0 - [EP])[I]}{(k_2[I] + k_3(K_M + [I]))(k_2 k_3 \frac{[I]}{k_2[I] + k_3(K_M + [I])} + k_4)} = [EB]$$

$$k_2 k_3 \frac{([E]_0 - [EP])[I]}{k_2 k_4[I] + k_3 k_4(K_M + [I]) + k_2 k_3[I]} = [EB]$$

Now, solving for [EP]:

$$\frac{d[EP]}{dt} = k_4[EB]$$

$$\frac{d[EP]}{dt} = k_2 k_3 k_4 \frac{([E]_0 - [EP])[I]}{k_2 k_4[I] + k_3 k_4(K_M + [I]) + k_2 k_3[I]}$$

Let us define X:

$$X = k_2 k_3 k_4 \frac{[I]}{k_2 k_4[I] + k_3 k_4(K_M + [I]) + k_2 k_3[I]}$$

$$\frac{d[EP]}{dt} = ([E]_0 - [EP]) * X$$

$$\frac{d[EP]}{([E]_0 - [EP])} = X * dt$$

$$\frac{d[EP]}{[EP]-[E]_0} = -X * dt$$

$$\int \frac{d[EP]}{[EP]-[E]_0} = \int -X * dt$$

With D as the constant that arises from evaluation of an indefinite integral:

$$ln([EP]-[E]_0) = -Xt + D$$

$$e^{ln([EP]-[E]_0)} = e^{-Xt+D}$$

$$[EP]-[E]_0 = e^{-Xt+D}$$

$$[EP] = [E]_0 + e^{-Xt+D}$$

$$[EP] = [E]_0 + e^{-Xt} * e^{D}$$

Since D is just a random, unknown constant, let us set e^D = F:

$$[EP] = [E]_0 + F * e^{-Xt}$$

Now, we know that at time t= 0, [EP] = 0:

$$0 = [E]_0 + F * e^{0}$$

$$-[E]_0 = F$$

$$[EP] = [E]_0 - [E]_0 e^{-Xt}$$

This means that when evaluating an inactivation time course and fitting it to an exponential, the k_{obs} is equal to X.

$$k_{obs} = k_2k_3k_4 \frac{[I]}{k_2k_4[I] + k_3k_4(K_M + [I])) + k_2k_3[I]}$$

$$k_{obs} = k_2k_3k_4 \frac{[I]}{(k_2k_3 + k_2k_4 + k_3k_4)[I] + k_3k_4K_M}$$

$$k_{obs} = \frac{k_2k_3k_4}{k_2k_3 + k_2k_4 + k_3k_4} * \frac{[I]}{[I] + \frac{k_3k_4K_M}{(k_2k_3 + k_2k_4 + k_3k_4)}}$$

k_{inact} is the left fraction in the equation directly above, as at infinite concentration of I, the right fraction will become 1, and k_{obs} will be equal to the left fraction. K_I is equal to the bottom right of the right fraction, as when the concentration of inhibitor equals this constant, the k_{obs} will be half of the k_{inact}.

II. Stopped-Flow Analysis of the Inhibition of BioA by 1.

Water used in all experiments was purified with a Millipore Super-Q system. Stopped flow experiments were performed using an Applied Photophysics stopped-flow instrument (model SX.18MV with the SX Pro-Data upgrade) at 25 °C. One syringe was filled with the stated concentration of BioA in 100 mM BICINE pH 8.6. The other syringe was filled with a solution derived from diluting a 20 mM solution of **1** in DMSO with 100 mM BICINE pH 8.6 to the specified concentration of **1**. All buffers were degassed prior to use. BioA was expressed as previously described[4] and **1** was synthesized as previously described.[5] Experiments were either monitored with a diode-array or a single wavelength detector. The concentration of BioA was kept below one-fifth of the concentration of **1**, establishing pseudo-first order conditions. The kinetic data was analyzed to extract reciprocal relaxation times with Applied Photophysics Pro-Data Viewer through fitting reaction time courses to summed exponential expressions. Simulations of the system with the obtained rate constants were performed with Tenua.

Analysis of transient kinetic data

The reaction time course for a series of first order or pseudo first order reactions can be fit by a sum of exponential expressions where the number of exponential terms is equal to the number of steps.[6,7] The time course is fit using nonlinear regression analysis to yield reciprocal relaxation times (RRTs) and amplitudes of the exponential terms. The RRT values are only equal to rate constants for individual steps in the reaction series if each step is irreversible. The order of magnitude of the RRTs in this case do not necessarily correlate with the order of steps in the reaction series. The presence of an irreversible step in the reaction series uncouples RRTs so that some of the RRTs may correlate with the rate constants for specific steps in the reaction series that occur after the irreversible step. For the reaction considered in this study, the second step is functionally irreversible, so one of the RRTs directly gives the rate constant for the final step in the reaction series. The presence of an irreversible step can often be detected by the lack of substrate concentration dependence on some of the RRT values. This is true because reversible steps couple RRT values such that a given RRT reflects more than one rate constant. In the general case, it is

necessary to extract the rate constants from experimental RRT values using expressions derived by integrating the series of differential rate equations that pertain to the proposed reaction steps. This leads to complex equations relating RRTs and rate constants. For example, for a two-step reversible binding reaction, the two RRTs are equal to the plus and minus roots of a quadratic equation containing all of the forward and reverse rate constants for the steps. Thus, neither of the RRTs correlates directly to one step of the series, but both will contain the second order rate constant for substrate binding and exhibit substrate concentration dependence. A useful simplification is possible if the substrate (or inhibitor) binding reaction initiates the reaction series and is fast compared with downstream reactions.[7,8] This allows it to reach an approximate equilibrium before the succeeding reactions occur. The specific criterion is that the reverse rate constant for binding reaction exceed the forward rate constant for the following reaction by >3 fold. If this is the case, then a plot of the fast RRT vs substrate concentration will be linear (which is what we observe) with the slope and intercept equal to the forward and reverse binding rate constants, respectively (equation 1). The plot of the slower RRT vs substrate concentration will be hyperbolic with the y-intercept equal to the reverse rate constant of the step following binding. The extrapolated maximum value of the hyperbola will be the sum of the forward and reverse rate constants for this reaction and the apparent K_D for the curve will be the K_D of the preceding binding reaction (equation 2, where A is the substrate or inhibitor).

$$RRT_{fast} \approx k_1[\mathrm{A}] + k_{-1} \quad (1)$$

$$RRT_{slow} \approx \frac{k_2[A]}{K_{D1}+[A]} + k_{-2} \quad (2)$$

If the K_D values determined from the two plots agree, then it suggests that the criteria for utilization of this simplification have been met and that one reaction directly follows the other. For the data analyzed in this study, the fastest and slowest RRTs give linear and hyperbolic plots vs **1**, respectively, and these plots yield similar values for the binding K_D (240 μM from equation 1, 180 μM from equation 2). The

concentration dependencies of all three observed RRTs allowed the reactions to be put in the correct sequence and the rate constants and K_D values to be extracted.

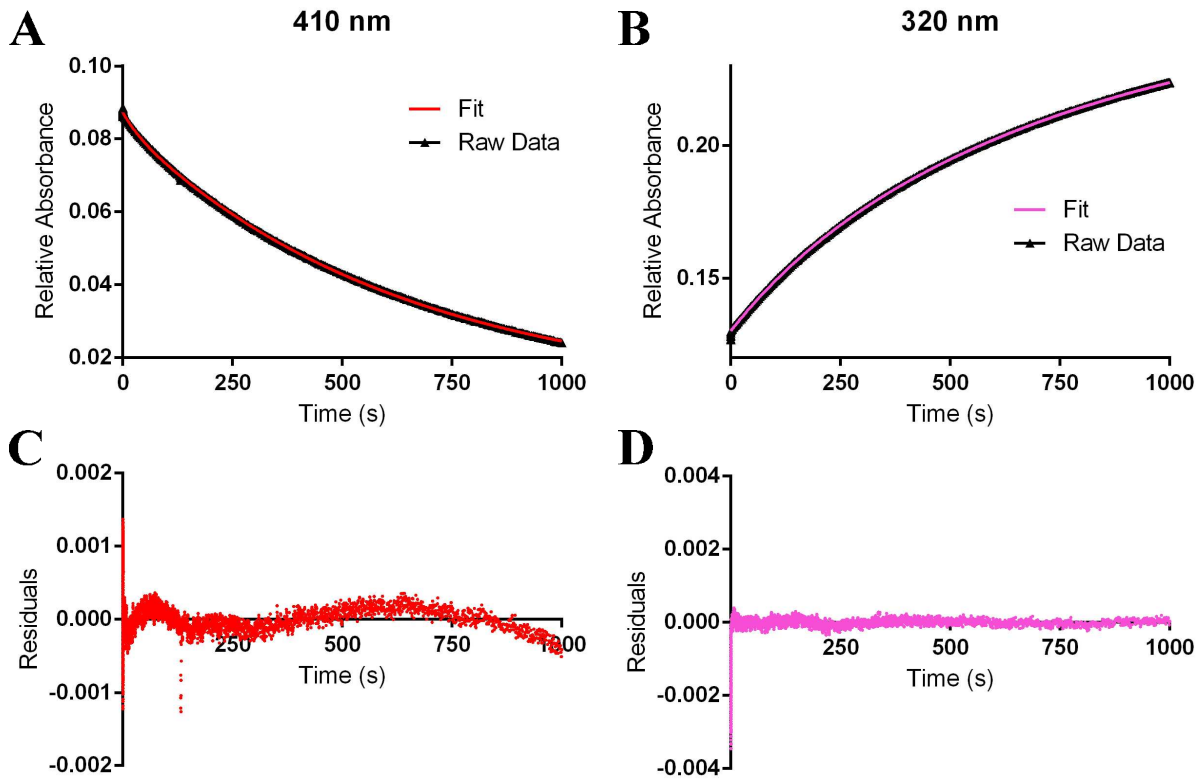

Figure S1. Traces obtained from spectrophotometrically monitoring the incubation of 12.5 μM BioA with 200 μM **1** in BICINE pH 8.6 at 23 °C. **A)** Trace obtained from monitoring at 410 nm for 1000 s with fitting. **B)** Trace obtained from monitoring at 320 nm for 1000 s with fitting. **C)** Residuals from fitting of part (A). **D)** Residuals from fitting of part (B),

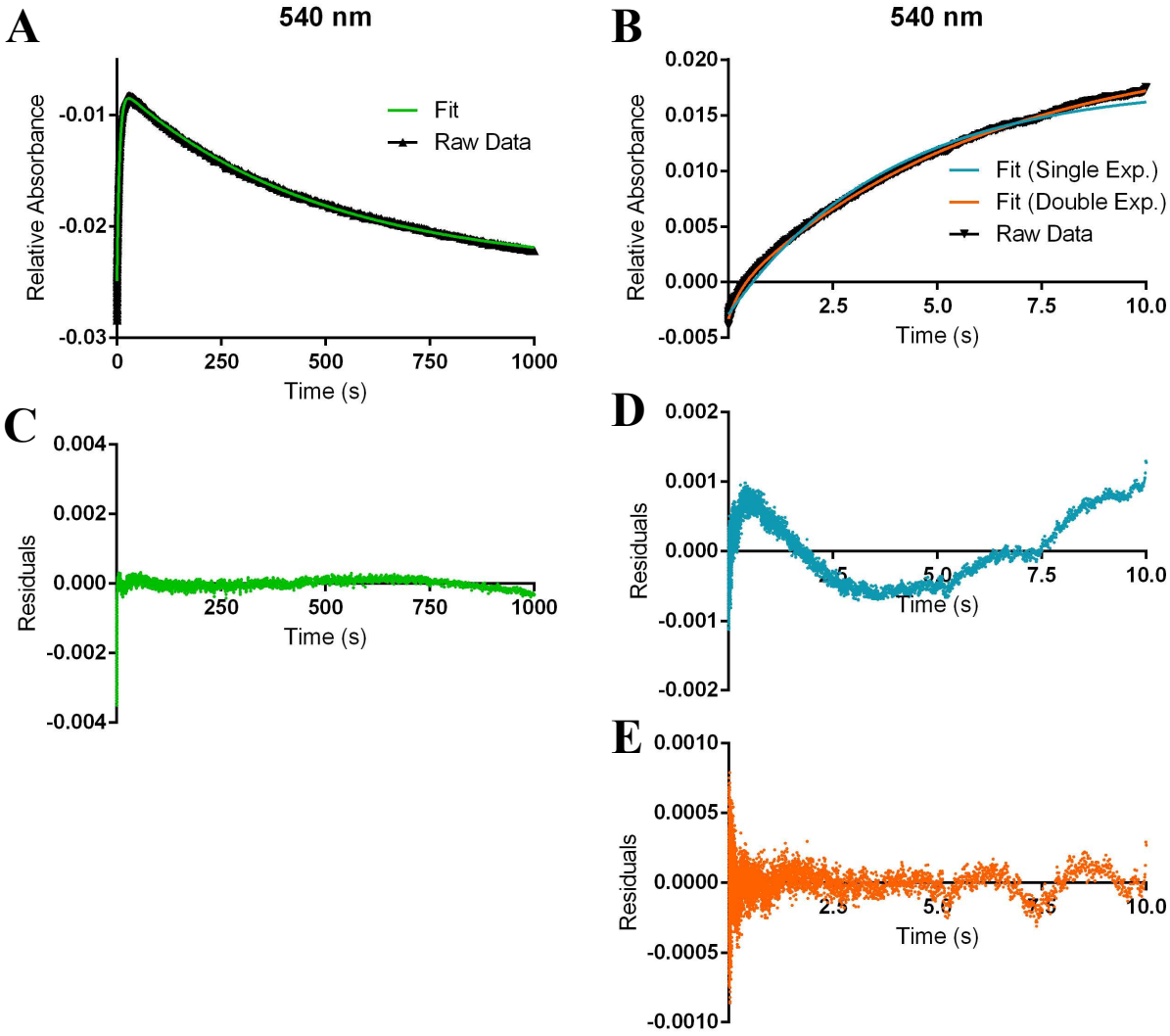

Figure S2. Traces obtained from spectrophotometrically monitoring at 540 nm the incubation of 12.5 μM BioA with 200 μM **1** in BICINE pH 8.6 at 23 °C. **A)** 1000 s trace with fitting. **B)** 10 s trace with fitting using one (blue) or two (orange) exponentials. **C)** Residuals from fitting of part (A). **D)** Residuals from single exponential fitting of part (B). **E)** Residuals from double exponential fitting of part (B).

Table S3. Reciprocal Relaxation Times from the Reaction of **1** with BioA. All times in are units of s^{-1}.

	Concentration of 1, μM					
	46.9	**62.5**	**93.8**	**125**	**187.5**	**200**
$\mathbf{1/\tau_1}$	n.d.	n.d.	n.d.	3.5±0.2	n.d.	4.1±0.3
$\mathbf{1/\tau_2}$	0.149±0.0014	0.149±0.0014	0.149±0.0009	0.146±0.0016	0.150±0.0012	0.146±0.007
$\mathbf{1/\tau_3}$	n.d.	n.d.	n.d.	0.0021±0.0001	n.d.	0.0027±0.0001
$\mathbf{1/\tau_4}$	n.d.	n.d.	n.d.	0.0006±0.0001	n.d.	0.0014±0.0001
	Concentration of 1, μM					
	300	**400**	**450**	**600**	**750**	**900**
$\mathbf{1/\tau_1}$	5.0±0.1	6.2±0.1	n.d.	8.0±0.2	n.d.	n.d.
$\mathbf{1/\tau_2}$	0.151±0.003	0.151±0.001	n.d.	0.150±0.002	n.d.	n.d.
$\mathbf{1/\tau_3}$	0.0032±0.0001	n.d.	0.0036±0.0001	0.0042±0.0004	0.0041±0.0002	0.0040±0.0005
$\mathbf{1/\tau_4}$	n.d.	n.d.	0.0012±0.0001	n.d.	0.0012±0.0003	n.d.

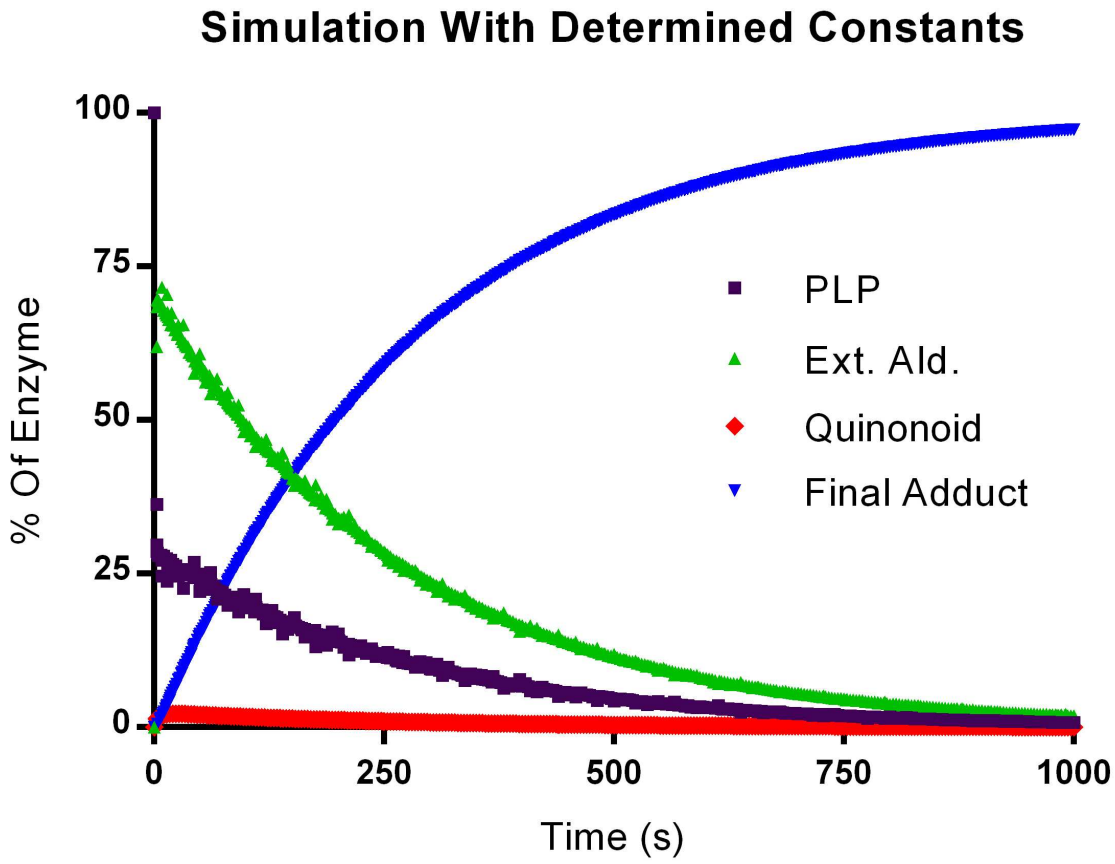

Figure S3. Simulation of the concentrations of each of the intermediates involved in inactivation of BioA by **1**. [BioA] = 12.5 μM, [**1**] = 600 μM.

Table S4. Comparison of Experimental Evidence and Simulation with Determined Constants

	Maximum Percentage of Quinonoid Reached
Experimental	2.6%
Simulation	2.2%

*[BioA] = 12.5 μM, [**1**] = 600 μM.

Experimentally, the time at which the maximum concentration of quinonoid is reached is determined by finding the maximum absorbance at 540 nm. This is likely a very accurate estimate, as the amplitude of the fastest RRT at 540 nm is very small compared to the amplitude of the other observed RRTs, indicating that the quinonoid itself accounts for a vast majority of the absorbance increase at 540 nm. The simulated time is just the time indicated by the simulation displayed in Figure S3.

Table S5: K_I and k_{inact} from Enzymatic Assay vs. Calculated Values from Rate Constant Determination

	K_I (μM)	k_{inact} (min^{-1})
Assay	520 ± 70	0.18 ± 0.01
Calculated	240	0.30

The calculated values use the values from Figure 2D with the formulas from entry 2 in Table 1 (k_4 set to 0).

III. Inhibition of BioA by 2.

Assay Procedure

50× DMSO solutions of inhibitor (**1** or **2**) (final concentrations 0, 200 μM, 400 μM, 700 μM, and 1 mM) were added to 1× buffer solutions of 100 mM Bicine (pH 8.6), 50 mM $NaHCO_3$, 1 mM $MgCl_2$, and 5 mM ATP. BioA (0.5 μM) was then added to each to well (total volume 50 μL) to initiate BioA inactivation.

In order to measure residual BioA activity, a coupled assay with BioD was used, which together with BioA converts 7-keto-8-aminopelargonic acid (KAPA) to dethiobiotin. This was accomplished by removing 5 μL aliquot of the initial solution at various incubation time points (2.5, 5, 10, 20, and 40 min) and adding to 95 μL of a reaction solution, containing saturating concentrations of all substrates and diluting the initial inhibitor 20-fold, ensuring no further inhibition. The final concentrations present in the reaction solution was 100 mM Bicine (pH 8.6), 50 mM $NaHCO_3$, 1 mM $MgCl_2$, 5 mM ATP, 5 mM SAM, 25 nM BioA, 2 μM BioD, 1 mM TCEP, and 25 μM KAPA.[9] The reaction solutions were run for 60 min (which remained under initial velocity conditions), then quenched with a solution of 500 nM biotin in 10% trichloroacetic acid. The dethiobiotin concentration was quantified by LC-MS/MS analysis with a gradient from 0-100% MeCN–H_2O containing 0.1% Formic Acid. Biotin was monitored through the m/z 243→200 transition and dethiobiotin was monitored through the m/z 213→170 transition. Assays were run in duplicate on multiple days. The negative control contained no inhibitor (DMSO only), and the positive control contained no BioA.

Data Analysis

The LC-MS/MS traces were analyzed by MultiQuant 2.0.2 to obtain the area under the curve (AUC) for both dethiobiotin (analyte) and biotin (internal standard). Then, the dethiobiotin AUC was divided by the biotin AUC, and this number was converted into a concentration using the standard curve. A plot was generated of preincubation time vs. percentage of BioA activity remaining, and curves for each concentration of inhibitor were fit to equation 3 with Graphpad Prism to obtain values for k_{obs} at each inhibitor concentration:

$$y = Ae^{-k_{obs}t} \quad (3)$$

In equation 3, y is the percentage of BioA activity remaining at time t, and A is the activity observed with no inhibitor (**Figure S4A**). The concentration of inhibitor was then plotted against the generated k_{obs} values, and this was fit to equation 4 with Graphpad Prism to provide values for k_{inact} and K_I (**Figure S4B**).

$$k_{obs} = k_{inact}\frac{[I]}{K_I+[I]} \quad (4)$$

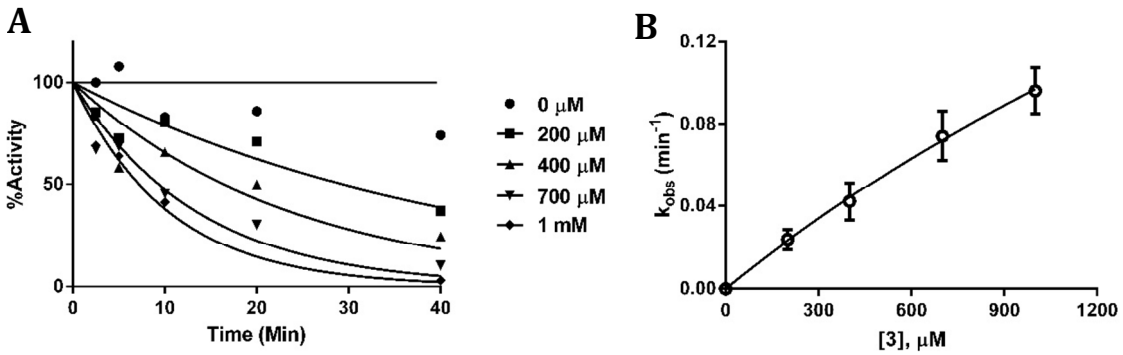

Figure S4. Determination of the k_{inact} and K_I values for inhibition of BioA by **2**. (A) Fitting inactivation curves to exponentials to obtain k_{obs} values. (B) Dependence of k_{obs} values on the concentration of **2**; fit to determine the k_{inact} and K_I values.

Unfortunately, we were unable to test concentrations of **2** higher than 1 mM due to solubility and assay constraints. The data in Figure S4 appears to fit a line quite well, allowing for a quite accurate estimate of the k_{inact}/K_I value. However, it also leads to difficulties in precisely projecting the k_{obs} at higher concentrations (Figure S5).

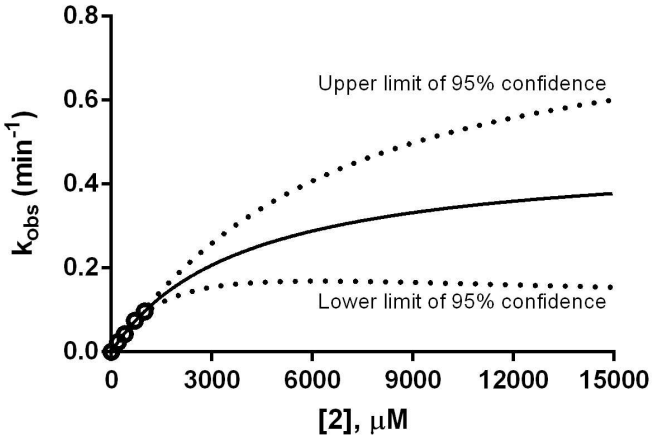

Figure S5. Projection of the curve shown in Figure S4 to higher concentrations of **2**. Includes upper and lower 95% confidence intervals.

IV. Crystallographic Data

Protein expression and crystallization

BioA protein was expressed and crystallized as previously described.[4,9] In brief, BioA crystals were obtained using the hanging drop vapor diffusion method. Drops consisted of 2 μL of 13 mg/mL protein, 1.5 μL of well solution, and 0.5 μL of a microseeding solution. Well conditions that yielded crystals included 100 mM HEPES pH 7.5, 100 mM $MgCl_2$, and 7% PEG 8k.

Protein-ligand complexes were obtained by soaking the crystals in mother liquor supplemented with 5.5 mM **3** for 1.25 h at rt. The crystals were then cryoprotected in mother liquor with 15% PEG 400, followed by flash vitrification in liquid nitrogen.

Data collection

Data for structure 5TE2 were collected at APS beamline 17-ID-B (IMCA-CAT) of Argonne National Labs equipped with a Dectris Pilatus 6M pixel array detector. The data were processed using AutoPROC.[10]

The structure was solved using Phaser[11] and the coordinates from 4W1X,[12] and it was refined using Phenix.[13] Visualization and modification was carried out using Coot.[14] Ligand restraints were calculated using JLigand.[15] Data processing and refinement statistics are available in Table S5, and omit maps are shown in Figure S6.

Insight from Structures

Structure 5TE2 is quite similar to 3TFU, the structure of the inactivated complex between **1** and BioA, with no large differences in alignment of the amino acid side chains within the active site. With the relatively small changes in K_I between **1** and **2** (likely 4-fold once the enantiomer of **2** is taken into account), we would not expect drastic changes in the binding mode between the two compounds. However, small changes in binding mode cannot be ruled out, which could certainly affect both the K_I and k_{inact} of **2**.

Table S6. Data processing and Refinement Statistics.

PDB ID code	5TE2
Source	APS 17-ID
Resolution (Å)	1.8
Space group	$P2_12_12_1$
Cell axis lengths (Å)	62.70 66.36 203.96
Data Processing	XDS
Resolution range (Å)	101.97-1.80
(high shell)	(1.808-1.800)
Observ. measured	5222874
(high shell)	(5023)
Unique reflections	79860
(high shell)	(744)
Average multiplicity	6.5
(high shell)	(6.8)
Completeness (%)	100.0
(high shell)	(99.7)
R_{merge}	0.055
(high shell)	(0.373)
Mean $<I/\sigma_I>$	22.0
(high shell)	(4.9)
Refinement Statistics	
Resolution range (Å)	41.61-1.80
Reflections used	75949
R_{free} reflections	3813
R_{work}	0.1679
R_{free}	0.1933
Non-hydrogen atoms	6914
Solvent waters	447
Mean B-factors (Å^2)	22.04
RMS deviations From Ideal Geometry	
Bond lengths (Å)	0.006
Bond angles (°)	0.862
Ramachandran plot outliers (%)	5 (0.6%)
MolProbity score	1.02

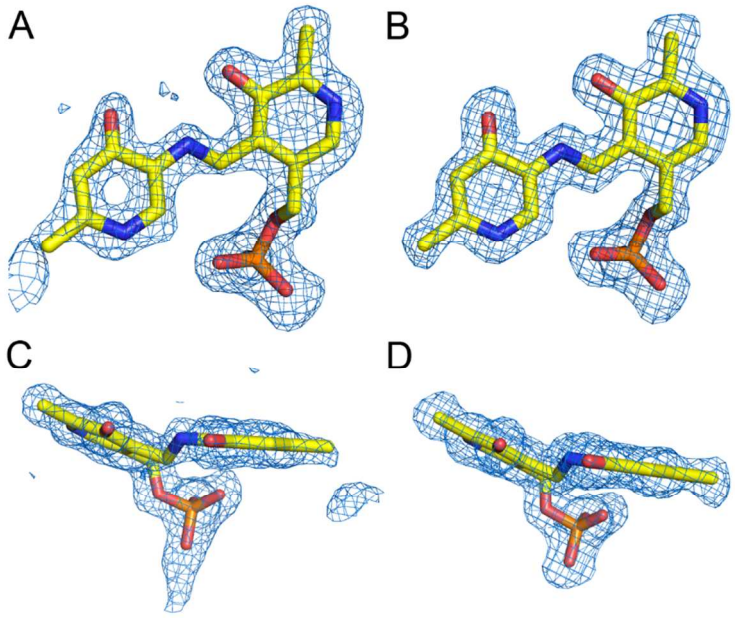

Figure S6. Omit maps (mF_o-DF_c, contoured at 3σ) for each covalent complex with compound **2** in structure 5TE2. For both ligands, some atoms are disordered and not modeled. **(A)** Chain A, showing formation of covalent bond **(B)** Chain B, showing formation of covalent bond. **(C)** Chain A, side view, showing planarity of adduct ring. **(D)** Chain B, side view, showing planarity of adduct ring.

V. NMR Spectra of 2.

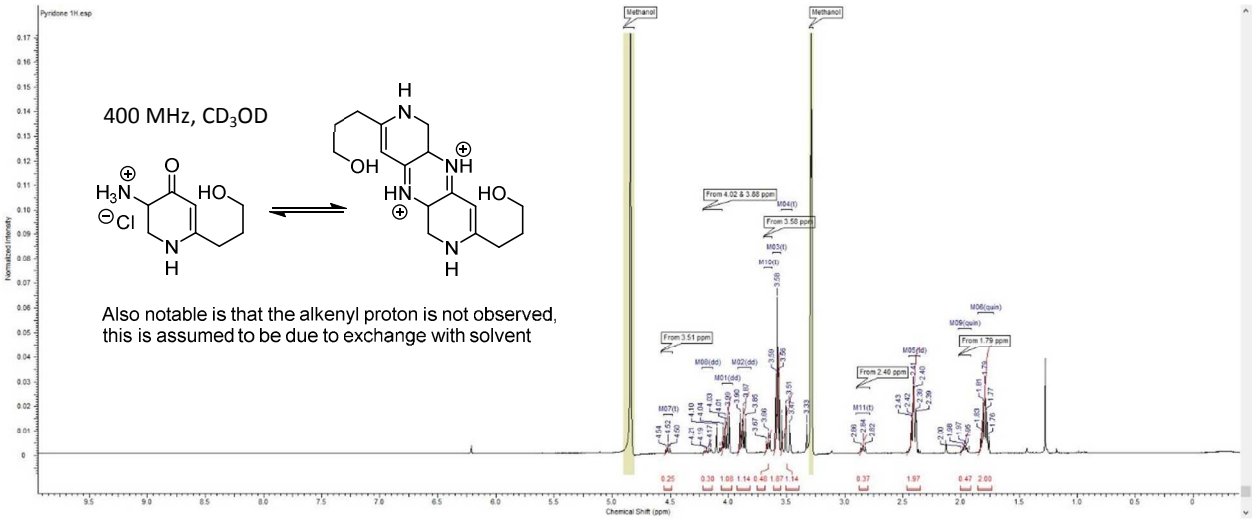

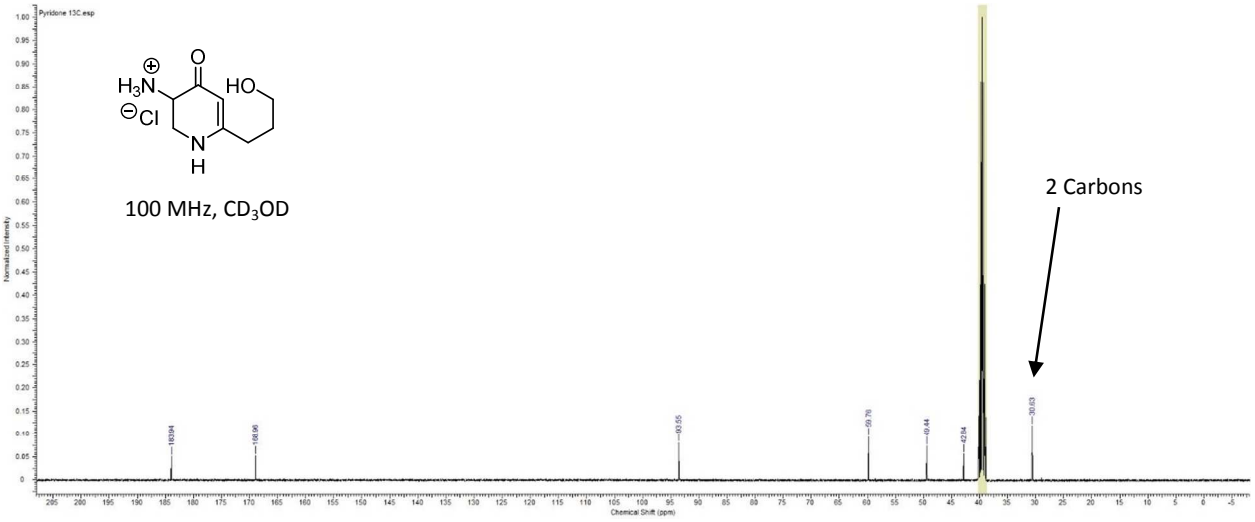

VI. References.

[1] Roest, H. *File:Enzyme Kinetics.pdf* Retrieved from https://commons.wikimedia.org/wiki/File:Enzyme_Kinetics.pdf# (accessed Nov 11, 2016).

[2] Copeland, R. H. *Evaluation of Enzyme Inhibitors in Drug Discovery: A Guide for Medicinal Chemists and Pharmacologists,* 2nd ed.; Wiley-Interscience: Hoboken, 2013.

[3] A similar method can be used to derive the K_I and k_{inact} values for the other mechanisms present in Table S1.

[4] Geders, T. W.; Gustafson, K.; Finzel, B. C.; *Acta Crystallogr. Sect. F Struct. Biol. Cryst. Commun.* **2012**, *68*, 596.

[5] Shi, C.; Geders, T. W.; Park, S. W.; Wilson, D. J.; Boshoff, H. I.; Abayomi, O.; Barry, C. E.; Schnappinger, D.; Finzel, B. C.; Aldrich, C. C.; *J. Am. Chem. Soc.* **2011**, *133*, 18194-18201.

[6] Verge, D. & Arrio-Dupont, M.; *Biochemistry* **1981**, *20*, 1210-1216.

[7] Groce, S. L.; Miller-Rodeberg, M. A.; Lipscomb, J. D.; *Biochemistry* **2004**, *43*, 15141-15153.

[8] Whittaker, J. W. & Lipscomb, J. D.; *J. Biol. Chem.* **1984**, *259*, 4476-4486.

[9] Wilson, D. J.; Shi, C.; Duckworth, B. P.; Muretta, J. M.; Manjunatha, U.; Sham, Y. Y.; Thomas, D. D.; Aldrich, C. C.; *Anal. Biochem.* **2011**, *416* (1), 27–38.

[10] Vonrhein, C.; Flensburg, C.; Keller, P.; Sharff, A.; Smart, O.; Paciorek, W.; Womack, T.; Bricogne, G.; *Acta Crystallogr. D Biol. Crystallogr.* **2011**, *67* (4), 293–302.

[11] McCoy, A. J.; Grosse-Kunstleve, R. W.; Adams, P. D.; Winn, M. D.; Storoni, L. C.; Read, R. J.; *J. Appl. Crystallogr.* **2007**, *40* (4), 658–674.

[12] Park, S. W.; Casalena, D. E.; Wilson, D. J.; Dai, R.; Nag, P. P.; Liu, F.; Boyce, J. P.; Bittker, J. A.; Schreiber, S. L.; Finzel, B. C.; Schnappinger, D.; Aldrich, C. C.; *Chem. Biol.* **2015**, *22* (1), 76–86.

[13] Adams, P. D.; Afonine, P. V.; Bunkoczi, G.; Chen, V. B.; Davis, I. W.; Echols, N.; Headd, J. J.; Hung, L.-W.; Kapral, G. J.; Grosse-Kunstleve, R. W.; McCoy, A. J.; Moriarty, N. W.; Oeffner, R.; Read, R. J.; Richardson, D. C.; Richardson, J. S.; Terwilliger, T. C.; Zwart, P. H.; *Acta Crystallogr. Sect. D* **2010**, *66* (2), 213–221.

[14] Emsley, P.; Cowtan, K.; *Acta Crystallogr. Sect. D* **2004**, *60* (12 Part 1), 2126–2132.

[15] Lebedev, A. A.; Young, P.; Isupov, M. N.; Moroz, O. V.; Vagin, A. A.; Murshudov, G. N.; *Acta Crystallogr. Sect. D Biol. Crystallogr.* **2012**, *68* (4), 431–440.